Chapter 2

“Modulation of electronic density states of carbon in expanded graphite *via* multifaceted Cu doped Co_2P particles for electrocatalytic hydrogen evolution reaction in aqueous acidic medium”

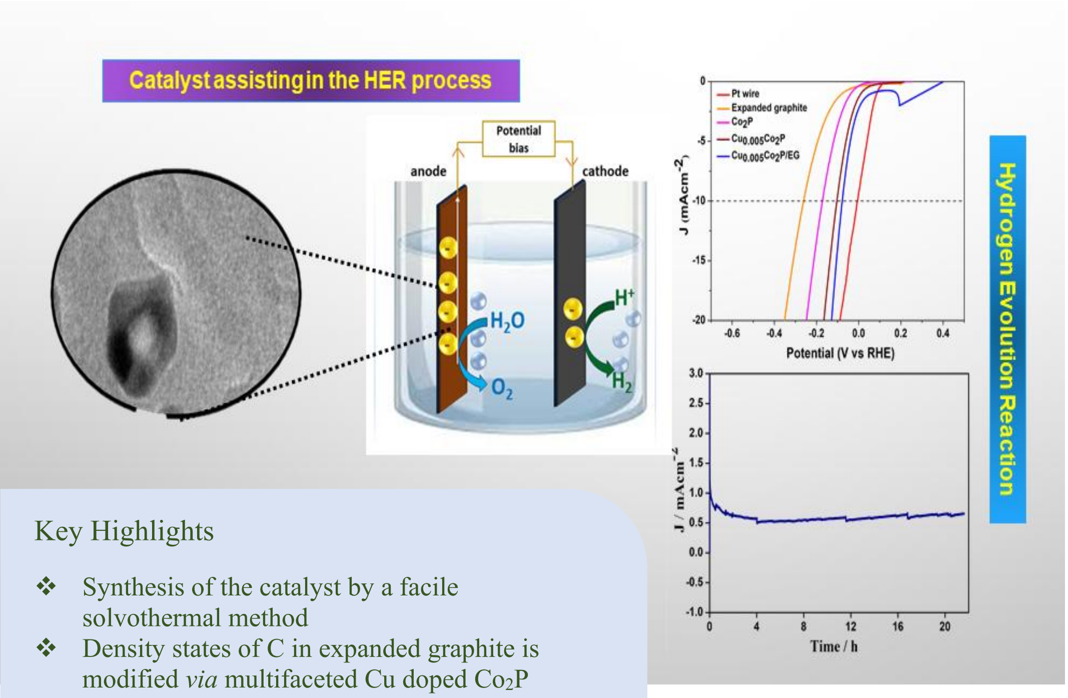

Key Highlights

- Synthesis of the catalyst by a facile solvothermal method
- Density states of C in expanded graphite is modified *via* multifaceted Cu doped Co_2P particle
- The catalyst requires overpotential value of 81 mV
- It endures long term stability in 0.5 M H_2SO_4 upto 21.6 h
- It retains its catalytic efficiency after 1000 cycles with negligible loss

2.1 Introduction

Hydrogen is considered as one of the crucial substitutes for fossil fuels and electrochemical water splitting is one of the efficient as well as sustainable methods of H_2 production. However, till now the best hydrogen evolution reaction (HER) catalyst is Pt. Due to less abudance and high cost of Pt water electrolyzer technique does not approve it as an effective electrocatalyst which is why intense research activities have been prompted towards the improvement of highly active HER catalysts based upon earth-abundant materials [1,2] *via* cost-effective methods. In the past few years, transition metal carbides, sulphides, phosphides, and selenides have drawn great attention as effective low cost HER catalysts with performances comparable to that of Pt [1].

It was discovered that HER proceeds through a similar pathway to that of hydrodesulphurization (HDS) reaction, where reversible adsorption/desorption of hydrogen on the catalyst surface is crucial for acquiring fast reaction kinetics. Due to this resemblance, transition metal phosphides (TMPs), previously employed as catalysts for HDS, launched a new avenue in the search of earth abundant metal catalysts for HER. Sabatier principle states that the H* adsorption free energy (ΔG(H*)) should neither be too strong nor too weak to pinpoint a good HER catalyst [3], and previous studies have corroborated the fact that TMPs, with a high P content, have the optimal ΔG(H*) values to become excellent HER catalysts [4]. Theoretical calculations have also revealed that the P ligand in TMPs, *via* the "ensemble effect", plays a pivotal role in releasing H_2 to drive HER efficiently. The ensemble effect stems from the electronegativity difference between P and the metal atoms, wherein the P atoms, being negatively charged, act as proton acceptors, and the metal atoms, being positively charged, act as hydride acceptors [5,6]. Among all TMPs, cobalt phosphides have been largely used due to their remarkable electrical conductivity and chemical

---

This part of the thesis is published in:

Lahkar, S., Ahmed, S., Bora, A., Mohan, K., Rohman, S.S., Guha, A.K., and Dolui, S.K. Modulation of electronic density states of carbon atom via multifaceted Cu doped Co_2P particle for robust and efficient electrocatalytic hydrogen evolution reaction in aqueous acidic medium. *Electrochimica Acta*, *455*:142378, 2023.

stability. The majority of the literature available focuses mainly on CoP. CoP has decidedly more advantages among the same metal phosphides: (i) a higher content of atomic P is thought to be more effective towards HER due to its ability to trap positively charged protons during electrolysis [7] and (ii) higher P content makes this phosphide more corrosion resistant [8]. In contrast, the activity of Co_2P has not been explored as extensively as that of CoP. But an important factor that needs to be given equal weightage is electrical conductivity. P atoms are highly electronegative, so they hinder electron delocalization, causing gradual reduction in conductivity with the increase in P content. In fact, high content of P may lead to a semi-conductive or even insulating state. Thus, higher concentration of P, actually curbs the movement of electrons which, in turn, decreases the H_2 production [5,9]. Accordingly, there needs to be a delicate balance between activity and conductivity to extract optimum results from the TMPs. In such a case, Co_2P can be considered as a suitable starting material to develop an efficient HER catalyst. Besides, the increased population of adsorbed hydrogen (H_{ads}) on the metal-metal bridge sites on Co_2P weakens the adsorption energies of hydrogen atoms, facilitating H_2 formation [10]. A few researchers have aspired to produce active electrodes from Co_2P as nanoporous Co_2P [11], Co_2P nanorods [12], carbon framework wrapped Co_2P on carbon cloth [13], Co_2P with oxygen incorporation [14], Co_2P encapsulated in N, P doped graphene [15], Co_2P nanoparticles grown on Co foil [16], etc. Huang *et al.* synthesized Co_2P nanorods where both Co and P in Co_2P acted as hydride and proton acceptor sites cooperatively rendering good HER efficiency in both acidic and basic solutions [12].

Regardless of all the success that has been achieved by TMPs as efficient HER catalysts, their performance has not been as satisfactory when it comes to practical applications. Consequently, doping with other elements has been considered to boost their activity. Literature study reveals that optimized $\Delta G(H^*)$ can be achieved by modulating the electronic structure of the catalyst *via* doping with metal (Fe, Co, Cu, Mn, Mo, Ni, etc.) or non-metal atoms (N, P, B, etc.) [17]. These dopants, especially the first-row transition metals, act as electrocatalytic activity promoters of TMPs by prompting redistribution of charges in the host phosphide, which ultimately decreases the $\Delta G(H^*)$ value [18]. The number of reports exploring the influence of Cu doping in cobalt phosphides in relation to the performance of HER is very rare. Yan *et al.* reported that the CoP electronic structure could be optimized by using Cu doping to aid the H* adsorption and desorption, and thus an optimum Cu content led to maximum efficiency in neutral-pH water splitting [19].

In order to further enhance the performance of a HER catalyst, structure engineering, in addition to composition engineering, also plays a pivotal role. Controlling the architecture of nano-scaled materials is very important as access to the surface-active sites to the reactants is quite crucial. Among various structures, hollow nanostructures hold promising possibility for various technical applications due to increased porosity, high surface area and easily accessible active sites, low mass density, efficient mass transport (diffusion of reactants and products), as well as enhanced electric and ionic conductive properties [20]. The more exposed active sites and open structure of hollow morphology provide a large electrode-electrolyte contact to improve the electrocatalytic performance far better than that of conventional bulky particles or thin films [21,22]. Thus, a lot of attention has been drawn to the hollow morphology. Callejas *et al.* introduced comparable catalytic activity of hollow Co_2P particles with morphologically equivalent CoP particles. They stated that the presence of the same element and the same morphology brought their efficiency into a comparable position [23]. Li *et al.* presented CoP nanocrystals with hollow morphology supported on reduced graphene oxide that rendered efficient catalytic activity towards HER. Hollow structure provided effective contact with the graphite layer, which led to higher charge transfer to the active sites [24].

It has been observed that the pioneering studies edge on designing metal-based catalysts to be the active sites for HER. But studies where carbon is the active site and such metal components possessing unique morphology acting as the auxiliary factor to enhance the HER efficiently are still scarce as carbon materials are mostly utilized as structural support for metal-based catalytic particles. Lately, it has been noticed that it is possible to serve carbon as active sites for HER *via* modulating the electronic density states of carbon atoms by transition metal elements [25], and this is the principal motivation of this chapter. In 2014, some research works claimed active carbon-transition metals (Fe, Co, and Ni) in HER systems for the first time. Till now, most of such studies have been confined to encapsulation of the metal catalysts in carbon nanotubes. In the present study, we aim to grab the advantage of intimate contact of multi-faceted hollow Cu doped Co_2P nanoparticles on expanded graphite (EG) sheets towards HER. More attachment sites and probably less corrosion of the active metals in acidic medium may occur due to the unique intercalated structure of

EG. Generally, thick carbon shells can obstruct the proper approach of mass transportation leading to poor electrocatalytic performance by the electrocatalyst, which is prevented by the use of EG in this work. The catalyst, Cu doped Co_2P@EG, is synthesized by *in-situ* solvothermal method and characterized with various analytical techniques. The electrochemical performance of the electrocatalyst is assessed by studying its polarization curves and Tafel plots. Durability and stability of the catalyst is evaluated by chronoamperometry and cyclic voltammetry (CV) tests, Mott-Schottky analysis presents the donor density of various catalysts for comparative study. A possible mechanism of HER on the catalytic surface is also discussed.

2.2 Materials and methods

2.2.1 Materials

All the chemicals including natural graphite flakes, cobalt acetate tetrahydrate, copper acetate monohydrate, oleylamine, trioctylphosphine (TOP), Nafion, ethanol, hexane, sulphuric acid (H_2SO_4) and nitric acid (HNO_3) purchased from Sigma-Aldrich were of analytical reagent grade purity and were directly used.

2.2.2 Methods

2.2.2.1 Synthesis of Expanded Graphite

EG was synthesized by a procedure adopted by Zheng *et al.* [28] Firstly, the natural graphite flakes were dried in a vacuum oven at 80°C for 24 h. The dried EG was then stirred with the mixture of concentrated H_2SO_4 and concentrated HNO_3 in a 4:1 (v/v) ratio for 24 h. Here, concentrated H_2SO_4 and HNO_3 served as the intercalating and the oxidizing agent respectively. The mixture was subsequently centrifuged and washed with distilled water until the pH became 6. Due to intercalation, an initial expansion step of the graphite layers occurred. The sample was then dried at 80°C in a vacuum oven for 24 h, followed by calcination at 900°C for 15 s in a muffle furnace. The pressure incurred due to the high calcination temperature caused swelling of the intercalate, leading to a second expansion step wherein an increase in the interlayer distance took place to give EG.

2.2.2.2 Synthesis of Cu doped Co_2P@EG

The catalyst was synthesized by a conventional solvothermal method. Typically, 12 mg of copper acetate, 0.257 g of cobalt acetate, 8 mL of oleylamine, and 50 mg of EG were mixed and stirred at 70°C in a 100 mL round bottom flask until a homogeneous dispersion was obtained. The dispersion was heated at 120°C in a heating mantle and TOP (20 mmol) was added. After that, the reaction setup was pumped under vacuum, and refilled with N_2 and temperature was maintained at 120°C for ½ h. Then, the reaction temperature was raised to 370°C and kept at that temperature for 10 min, after which a black-coloured precipitate was obtained. After bringing down to room temperature the sample was washed multiple times by a solvent mixture of hexane and ethanol (V_{hexane}:$V_{ethanol}$ = 1:3). The obtained hybrid catalyst, termed $Cu_{0.005}Co_2P$@EG was then dried under vacuum at room temperature. The notations, Cu doped Co_2P@EG and $Cu_{0.005}Co_2P$@EG have been used interchangeably throughout the paper.

The whole process was repeated without the addition of EG to obtain Cu doped Co_2P. Here we synthesized three different compositions of Cu doped Co_2P with varying Cu:Co molar ratios (Cu:Co = 0.03, 0.05, 0.1), and denoted as $Cu_{0.003}Co_2P$, $Cu_{0.005}Co_2P$, and $Cu_{0.01}Co_2P$ respectively.

For further comparative study, Co_2P was also synthesized by the same procedure without the addition of EG and copper acetate.

2.2.3 Characterization and measurements

The prepared samples were characterized by XRD, FTIR, SEM, TEM, EDX and XPS analyses. The electrochemical behaviour of the samples was studied with a standard three electrodes cell compartment where a carbon electrode and a silver/silver chloride electrode were used as the counter and the reference electrode respectively. The working electrode was prepared by dispersing 2 mg of the synthesized electrocatalyst in 0.1 mL 0.5 wt% Nafion solution. 0.002 mL of this prepared dispersion was coated onto ~ 0.07 cm^2 surface area of glassy carbon electrode (GCE, radius 1.5 mm) by drop casting and then naturally dried at room temperature. 0.5 M H_2SO_4 aqueous solution was used as the electrolyte for all the electrochemical measurements.

The entire experimental procedure is illustrated in Scheme 2.1.

Step 1: Synthesis of expanded graphite

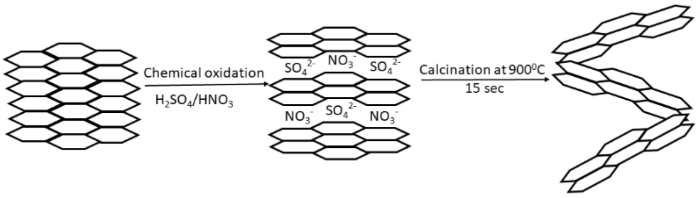

Step 2: Synthesis of the product Cu doped Co_2P@EG

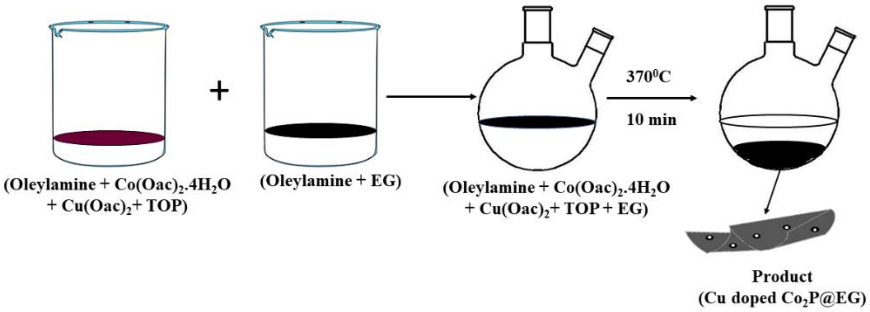

Step 3: Preparation of the working electrode

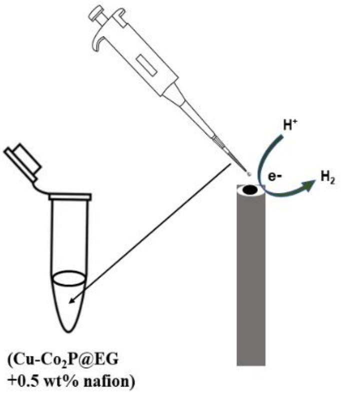

Scheme 2.1 Experimental scheme of synthesis of Cu doped Co_2P@EG composite and the drop casting process.

2.2.4 Computational details

The structure of EG, EG encapsulated Co_2P and Cu doped Co_2P@EG were fully optimized at PBE1PBE/def2-TZVP level [29]. Harmonic vibrational frequency calculations were conducted at the same level of theory to realize the nature of the stationary state. All the structures were turned out to be at their local minima with all real values of the Hessian matrix. The free energies of the intermediates were acquired by $\Delta G(H^*) = \Delta E(H^*) + \Delta ZPE\text{-}T\Delta S$, where $\Delta E(H^*)$, ΔZPE and ΔS is the binding energy, zero-point energy change, and entropy change of H_{ads} respectively. All these calculations were carried out using Gaussian16 suite of program [30].

Projected density of states (PDOS) was assessed by Multiwfn program code [31].

2.3 Results and discussion

2.3.1 XRD analyses

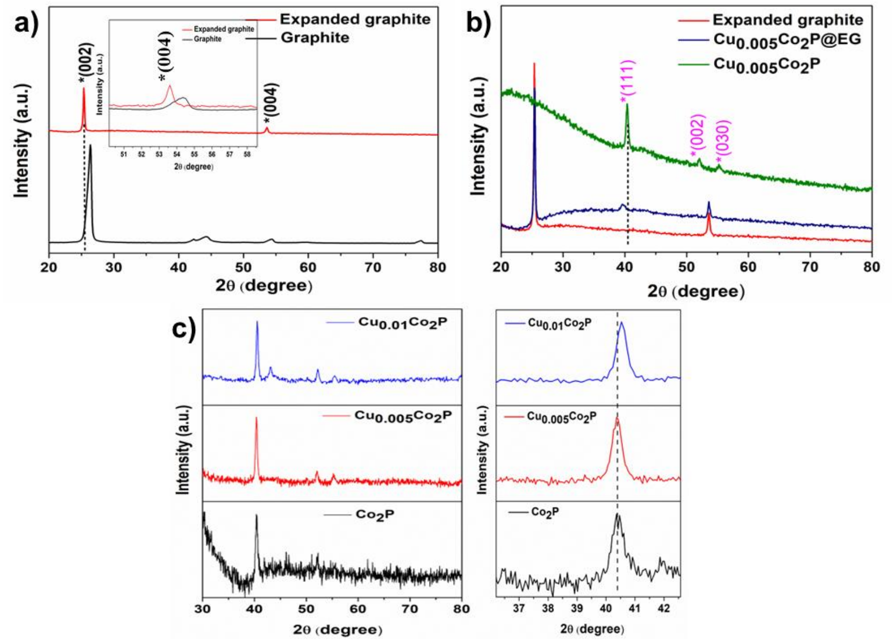

Figure 2.1 XRD patterns of (a) natural graphite flakes and EG, (b) EG, $Cu_{0.005}Co_2P$, and $Cu_{0.005}Co_2P$@EG, (c) Co_2P, $Cu_{0.003}Co_2P$, $Cu_{0.005}Co_2P$ and $Cu_{0.01}Co_2P$ (right part is the magnified image for the significant (111) plane of the respective composites.

The crystal structures of the samples were investigated by XRD analysis. From **Figure 2.1(a)**, two significant intense peaks at $2\theta = \sim 26°$ (002) and ~54° (004) suggest the crystalline nature of both natural and expanded forms of graphite [32]. However, in case of EG, the decrease in intensity of both the XRD peaks is indicative of increasing surface area and porous nature of EG. Comparison of both leads to the outcome that the peaks corresponding to (002) and (004) planes for EG shift towards the lower angle. Leveraging Bragg's law, $\lambda = 2d\sin\theta$ (where λ is the wavelength, d is the interlayer spacing and θ is the angle between the individual atomic planes), it is definite that shifting explicates the increase of interlayer spacing. In **Figure 2.1(b)**, XRD pattern for Cu doped Co_2P presents a distinctive intense peak at 2θ = 40.6° and two broad peaks at 2θ = 52.5° and 55.8° corresponding to (111), (002), and (030) crystal planes of hexagonal Co_2P respectively [33]. No characteristic peak pertaining to Cu signifies the successful doping of Cu in Co_2P. The significant (111) diffraction peaks in Co_2P, $Cu_{0.003}Co_2P$, and $Cu_{0.005}Co_2P$ are consistent at the same position. However, upon increasing Cu concentration in $Cu_{0.01}Co_2P$ the lattice of Co_2P gets compressed and along with other Co_2P peaks an additional intense peak corresponding to cubic Cu (111) plane implies that saturation and excess of Cu leads to formation of Cu nanocluster (**Figure 2.1(c)**). Diffraction pattern for Cu doped Co_2P@EG displays consistent peaks at 2θ=26° and 54° with slight right shifting suggesting the growth of Cu doped Co_2P particles on EG sheet. The peak at 40.6° corresponding to distinctive (111) plane of hexagonal Co_2P structure gets left shifted which may be due to lattice expansion as a result of some defect sites. This may be involved in modulation of surface electronic structure that favours the electrocatalytic performance. The dominating (002) and (004) plane at the same position of the synthesized composite suggests the retention of EG structure and also implies the key role of carbon in the catalytic activity. However, all the diffraction peaks get broadened due to amorphous nature of the catalyst and therefore peaks corresponding to (002) and (030) planes are not distinct. The broadening of diffraction peaks signifies surface area increment of the catalyst. Nonetheless, the diffraction spectrum does not display any new peak, indicating the high purity of the synthesized catalyst.

2.3.2 FTIR spectra analyses

The interaction between Cu doped Co_2P and EG was further investigated *via* FTIR spectra analysis (**Figure 2.2**). Both the spectra display a wide absorption band at 3450 cm^{-1} which can be assigned to the O–H stretching mode due to the moisture adsorption on the catalyst surface. The frequency bands at 2926 and 2852 cm^{-1} are due to aliphatic character of the C–H bonds. The band at 1636 cm^{-1} may be due to stretching vibrations of carboxylic group/aromatic ring stretching vibrations of the carbon moiety [31]. The additional peak at 1078 cm^{-1} of Cu doped Co_2P@EG is characteristic of C–P bond which ensures successful composite formation [34].

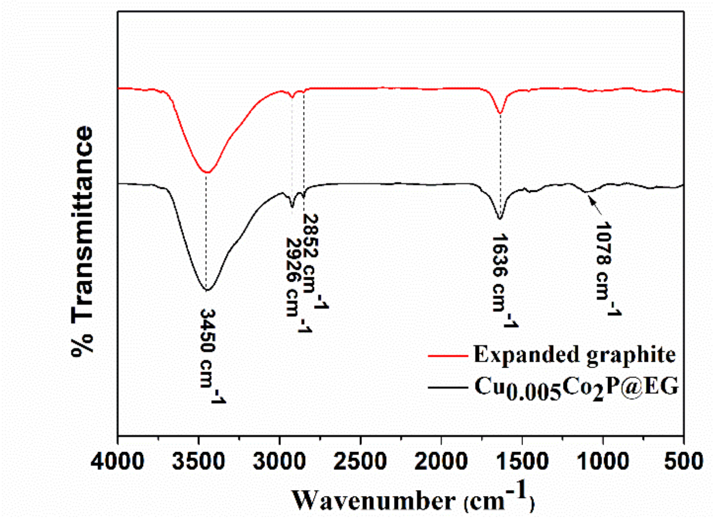

Figure 2.2 FTIR spectra of EG and $Cu_{0.005}Co_2P$@EG.

2.3.3 Morphological analyses

Surface morphology of graphite before and after expansion is shown in the SEM images in **Figure 2.3(a-c)**. The natural graphite flakes possess tightly stacked layered structure whereas exfoliation of graphite sheets leads to a porous hive-like structure with increased surface area where spacing between the layers is well-defined. In **Figure 2.3(d)**, Cu doped Co_2P particles are observed on EG sheet. Growth of multi-faceted hollow Cu doped Co_2P particles on the hive structure of EG is obvious from TEM images (**Figure 2.3(e)**). Formation of these hollow Cu doped Co_2P particles is a result of the well-known nanoscale Kirkendall effect (**Figure 2.3(f)**). Due to the difference in chemical potential and concentration gradient, Co^{2+} ions slow down the inter diffusion of P^{3-} ions which results in the core vacancies merging into a hollow void [35,36]. From the TEM images, it is observed that all the particles have average diameter of ~37 nm which is obtained from the particle distribution curve (inset of **Figure 2.3(e)**) due to the presence of a core void. The maximum surface contact of the hollow Cu doped Co_2P particles with EG sheets leads to the formation of new energy levels around the carbon atoms to generate new active sites. The charge transfer to the active sites occurs at a much faster rate in the interconnected thin EG sheets with lower contact electrical resistance than in the stacked graphite sheets probably due to percolation [37], which accredits another beneficial feature for this active HER. Layered EG enhances the HER due to weak interlayer van der Waals interactions, allowing the ultrathin nanosheets to aid in active site loading and adsorption of intermediates.

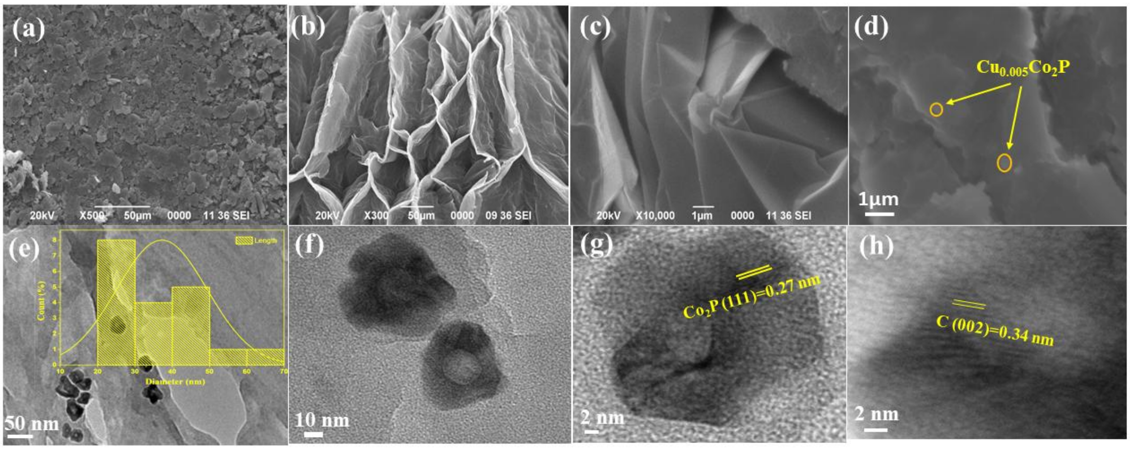

Figure 2.3 SEM images of (a) graphite, (b, c) EG and (d) $Cu_{0.005}Co_2P$@EG; (e, f) TEM images showing hollow Cu doped Co_2P particles reside in the hive structure of EG at different resolutions; (g, h) HRTEM images of the composite with significant (111) plane of Co_2P particles and (002) plane corresponding to EG

Moreover, the hive-like structure of EG may be effective in prevention of agglomeration and corrosion resistance of nanoparticles in acidic environment to some extent to promote longevity of the catalytic performance. The high-resolution TEM (HRTEM) images of Cu doped Co_2P@EG, (**Figure 2.3(g, h)**) show the separation of lattice fringes by 0.27 nm that corresponds to (111) plane of Co_2P and 0.34 nm that corresponds to (002) plane of EG which are well in agreement with the XRD data in **Figure 2.1(b)**.

2.3.4 EDX spectral analysis and elemental mapping images

From the EDX spectrum (**Figure 2.4 (a)**), the obtained weight percent ratio of 4.2:2.5 confirms the stoichiometry of the Co_2P phase in the composite. The spectrum also confirms Cu, Co, P, and C elements in the composite in the expected ratios with negligible impurities. The elemental mapping (**Figure 2.4 (b-d)**) demonstrates that all the elements are uniformly distributed.

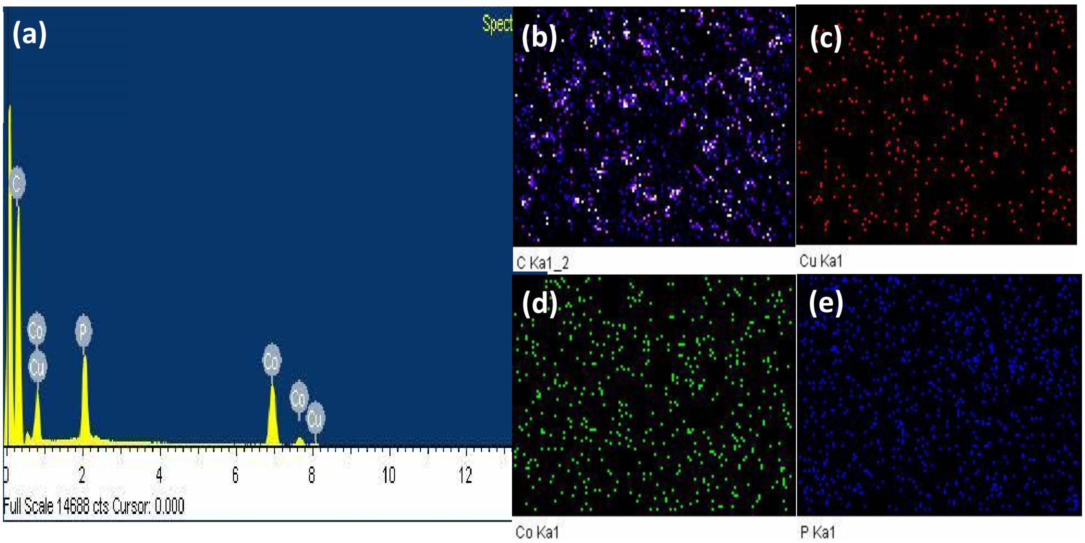

Figure 2.4 (a) EDX spectra of $Cu_{0.005}Co_2P$@EG and elemental distribution of (b) C, (c) Cu, (d) Co, and (e) P.

2.3.5 XPS analysis

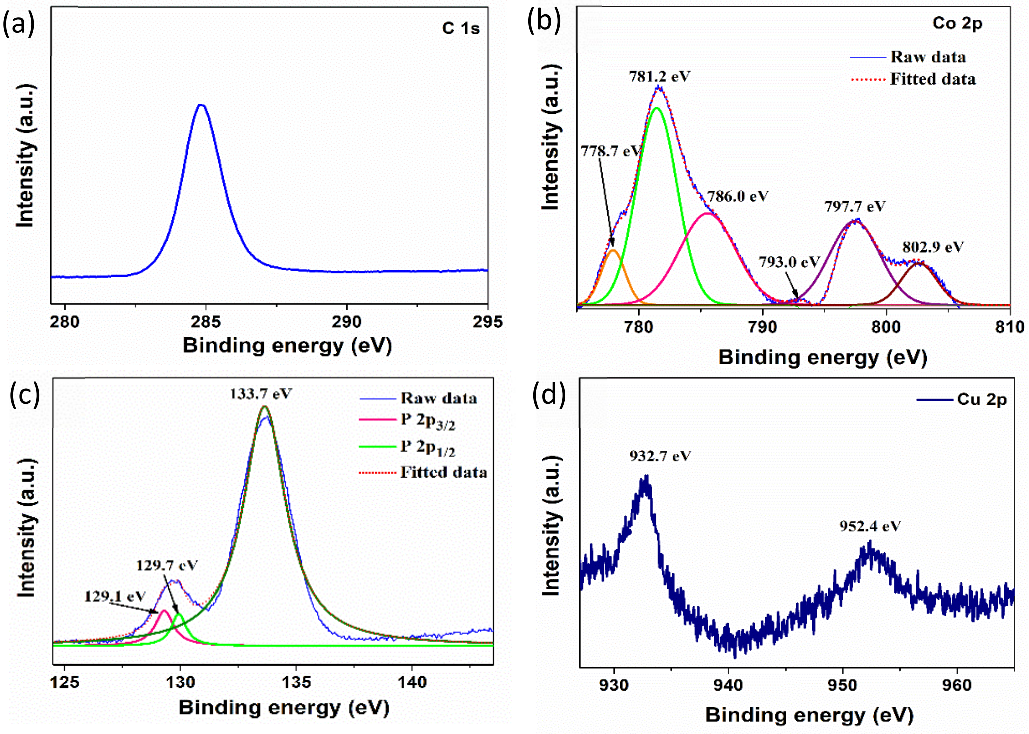

Figure 2.5 High-resolution XPS spectra of (a) C 1s, (b) Co 2p, (c) Cu 2p and (d) P 2p of $Cu_{0.005}Co_2P$@EG respectively.

The elemental valence state and the surface chemical composition of the $Cu_{0.005}Co_2P$@EG catalyst were characterized by XPS analysis. From the high-resolution survey spectra (**Figure 2.5 (a)**), a single distinguished peak in C 1s orbit was observed at 285 eV corresponding to the sp^2 carbon atoms of EG. XPS spectrum of Co 2p orbital (**Figure 2.5 (b)**) in $Cu_{0.005}Co_2P$@EG exhibits two peaks positioned at 778.7 eV and 781.2 eV with a satellite peak at 786.0 eV which can be ascribed to Co $2p_{3/2}$ energy level, and two peaks located at 793 eV and 797.7 eV with a satellite peak at 802.9 eV can be attributed to the Co $2p_{1/2}$ energy level. The peaks at 781.2 eV and 797.7 eV reflects the presence of oxidized Co^{2+} species. The two apparent satellite peaks are assigned to the shakeup excitation of the high-spin Co^{2+} ions. Cu 2p spectrum in **Figure 2.5 (c)** exhibits binding energy values of 932.7 eV and 952.4 eV which are attributed to Cu $2p_{3/2}$ and Cu $2p_{1/2}$ respectively. Co−P of Co_2P can be determined by the P 2p spectrum (**Figure 2.5 (d)**) of the $Cu_{0.005}Co_2P$@EG hybrid catalyst. Two peaks are observed at 129.1 and 129.7 representing the P $2p_{3/2}$ and P $2p_{1/2}$ energy levels in Co_2P respectively along with a sharp peak at 133.7 eV allocated to surface oxidization of P species in P-C due to air contact [30]. The survey confirms significant blue shifting of the binding energy of Co $2p_{3/2}$ in the catalyst as compared to that of pure Co metal (778.1 eV). The energy of P 2p3/2 (129.1 eV) in the catalyst is also lower than that of pure P element (130.0 eV), which pinpoints that the charge density near Co is apparently transferred leading to the existence of cationic Co and anionic P species.

2.3.6 Electrochemical analysis

To obtain information on the HER activity of the prepared catalyst, electrochemical characterization was performed using a three-electrode set-up in 0.5 M H_2SO_4 solution at room temperature. The polarization curves (J-V plots) were obtained by sweeping the potential from 0 to -0.6 V (*vs* Ag/AgCl) with a sweeping rate of 50 mV sec^{-1}. In this study, all the potentials were measured with standard calomel electrode (SCE) and then modified to reversible hydrogen electrode (RHE) applying the equation 2.1.

$$E(RHE) = E(SCE) + 0.0591\ pH + 0.1976\ V \qquad \text{equation 2.1}$$

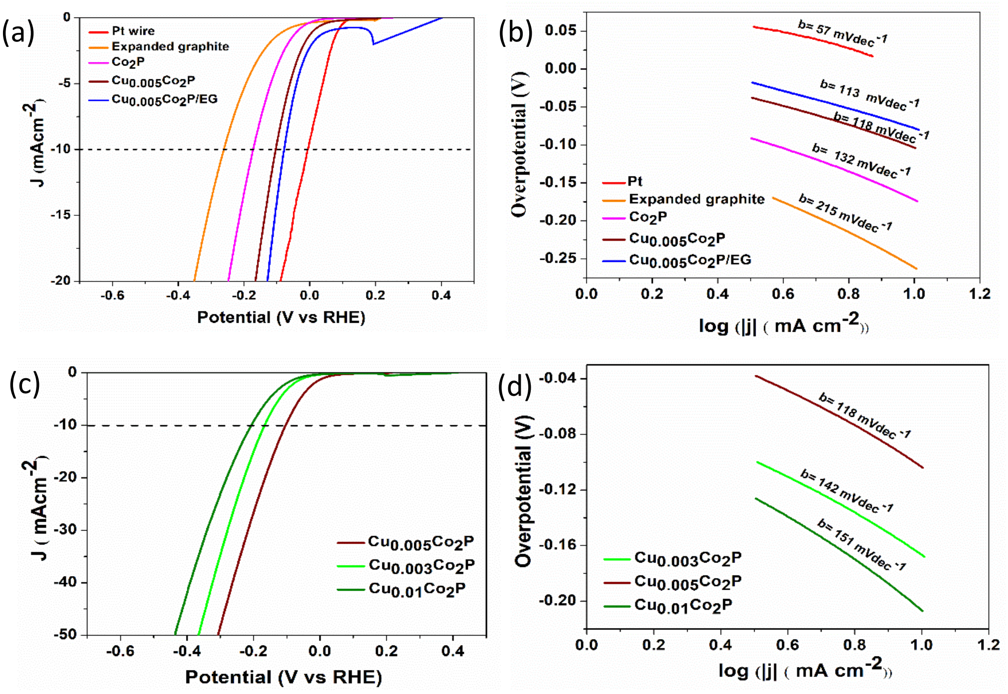

Figure 2.6 Electrocatalytic performances of the catalysts in 0.5 M H_2SO_4 in terms of (a,c) their polarization curves and (c, d) Tafel plots

From the non-zero cathodic current measurements (**Figure 2.6 (a)**), it is observed that Cu doped Co_2P@EG requires only -81 mV overpotential (η_{10}) to achieve the benchmark current density of 10 mA cm^{-2} which remarkably get reduced than that of $Cu_{0.003}Co_2P$ (-164 mV), $Cu_{0.005}Co_2P$ (-104 mV), $Cu_{0.01}Co_2P$ (-205 mV), Co_2P (-174 mV), EG (-262 mV) with the same catalyst loading and comparable to that of Pt electrode, the value of which is ~0 V vs RHE. This improvement comes from the strong contact of the Cu doped Co_2P particles with the EG sheets which facilitates fast charge transfer from the nanoparticles to the active catalytic sites *via* electronic coupling. EG acts as interconnected network and also stands as a fine support for highly dispersed Cu doped Co_2P. From previous studies, it has been observed that once coupled with graphene, Co-terminated Co_2P becomes energetically favourable with a binding energy value of 1.58 eV than that of P- terminated Co_2P with binding energy of 0.67 eV [38,39]. Thus, strong Co-C covalent bond formation eases rapid electron transfer from Co_2P to the active carbon sites. Electronegativity difference between the non-precious metal and carbon leads to a charge transfer from the metal to carbon when they both interact with each other. This facile electron transfer increases the charge density around the carbon atom. Moreover, presence of two Co atoms in per metal moiety may led to better electron transfer. When Co and C come in contact, then emergence of new energy levels around carbon directs the location of band centers of the filled states of C-H bond (sum of C_{2p} and H_{1s}) in the lower energy region (**Figure 2.12**) than that of EG. The result causes the stabilization of H_{ads} atoms on the surface of EG near Co_2P moiety. Furthermore, the presence of P atoms could effectively inhibit the electro-oxidation of active catalytic carbon sites [40] and most probably promote hydrogen desorption as the presence of anionic P was confirmed in XPS analysis that favours HER.

For maximum catalytic efficiency from the composite the role of auxiliary Cu doped Co_2P particle is quite important. The more conductive the particle the easier will be the charge transfer to the active site. Hence, we also checked the catalytic activity of Cu doped Co_2P alone by tuning the dopant content. Doping of Cu into Co_2P generates new electronic states within the wide band gap of Co_2P [19]. Due to this effect, electrons can easily reach the surface-active sites. Up to a specific dopant concentration (in this case, $Cu_{0.005}Co_2P$), the catalytic performance keeps on increasing but after reaching an optimum composition further increase of Cu leads to aggregation that may cover the active sites and thus deteriorate the integral catalytic activity (**Figure 2.6 (c, d)**). Copper nanoclusters are found to be formed at Cu:Co ratio of 0.01, which drastically increases the Ohmic drop.

The kinetics and the mechanistic pathway of HER were analyzed by Tafel slopes, an inherent intrinsic property of the catalysts which is derived by fitting the linear portion of polarization curve data to equations 2 (a, b).

$$\ln J = \ln J_0 + (-\alpha_c nF / RT)\, \eta \qquad \text{equation 2.2 (a)}$$

$$2.303\, RT / -\alpha_c nF = b \text{ (Tafel slope)} \qquad \text{equation 2.2 (b)}$$

where J is the current density and J_0 is the exchange current density, α_c is the charge transfer coefficient for the cathodic potential, n is the number of electrons transferred, F is Faraday's constant, R is the ideal gas constant, T is the temperature in Kelvin and η is the iR-corrected potential. $Cu_{0.005}Co_2P$@EG shows a Tafel slope value of 113 mV dec^{-1} that is lower than those of $Cu_{0.003}Co_2P$ (142 mV dec^{-1}), $Cu_{0.005}Co_2P$ (118 mV dec^{-1}), $Cu_{0.01}Co_2P$ (151 mV dec^{-1}), Co_2P (132 mV dec^{-1}) and EG (215 mV dec^{-1}) (**Figure 2.6 (b, d)**). Smaller Tafel slope suggests faster HER rate and smaller energy requirement for the HER.

Electrocatalytic HER proceeds *via* two possible routes:

The adsorption reaction (Volmer step) with the Tafel slope of about 120 mV dec^{-1}.

$$H^+ + e^- \rightarrow H_{ads} \qquad \text{equation 2.3}$$

And

the electrochemical desorption reaction (Heyrovsky step) with the Tafel slope of ~ 40 mV dec^{-1} or

$H_{ads} + H^+ + e^- \rightarrow H_2$ equation 2.4 (a)

the chemical desorption and recombination reaction (Tafel step) with a Tafel slope of ~ 30 mV dec^{-1}.

$H_{ads} + H_{ads} \rightarrow H_2$ equation 2.4 (b)

Combination of two of these steps as Volmer-Heyrovsky (equation 2.3 with equation 2.4 (a)) or Volmer-Tafel (equation 2.3 with equation 2.4 (b)) mechanism led to the formation of molecular hydrogen [27,41,42] Tafel slope analysis exhibits a value of 113 mV dec^{-1} (**Figure 2.6 (b)**) for $Cu_{0.005}Co_2P$ /EG that falls in between 40 and 120 mVdec^{-1}. This indicates that the HER kinetics follows Volmer-Heyrovsky mechanism and the removal of hydrogen from water molecule on the surface of electrode (Volmer step) is the rate-limiting step [27]. The strength of H_{ads}-active catalytic surface bond likely controls the overall HER kinetics. Among EG, Co_2P and $Cu_{0.005}Co_2P$ /EG, $Cu_{0.005}Co_2P$ /EG exhibits the lowest Tafel slope value which is consistent with our theoretical calculation. Density functional theory (DFT) calculation results in a lower positive $\Delta G(H^*)$ value of (0.12 eV) for $Cu_{0.005}Co_2P$ /EG compared to that of EG, Co_2P explains the ease of H_{ads} formation on the catalytic surface that describes better interaction between H_{ads} and the surface. The result indicates that although the catalytic activity is not spontaneous but it proceeds with much lower overpotential compared to the other mentioned experimental catalysts. The plausible mechanism of HER on $Cu_{0.005}Co_2P$@EG is as follows:

$H_3O^+(aq) + e^- + C^* \rightarrow CH_{ads} + H_2O$ (Volmer step)

$CH_{ads} + H_3O^+(aq) + e^- \rightarrow H_2(g) + H_2O(l) + C^*$ (Heyrovsky step)

C* stands for the active carbon sites of EG and H_{ads} stands for the adsorbed hydrogen on the active sites.

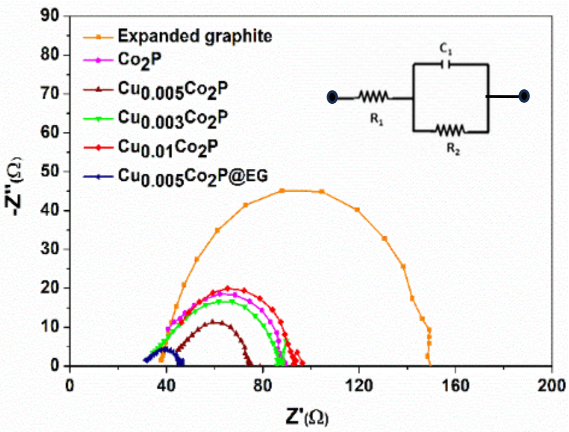

Figure 2.7 Nyquist impedance plots of various catalysts (the inset shows the equivalent circuit diagram)

The interfacial charge transfer resistance was studied by evaluating electrochemical impedance spectroscopy (EIS) analysis for the catalysts at a steady overpotential of -80 mV *vs* RHE within the frequency range from 100 mHz to 10 kHz. The values of the charge-transfer resistance (R_{ct}) calibrated from the Nyquist plots (**Figure 2.7**) are 15 Ω, 49 Ω, 30 Ω, 58 Ω, 54 Ω and 111 Ω for $Cu_{0.005}Co_2P$@EG, $Cu_{0.003}Co_2P$, $Cu_{0.005}Co_2P$, $Cu_{0.01}Co_2P$, Co_2P and EG respectively. In the inset circuit diagram of **Figure 2.7**, R_2, R_1, and C_1 represent the interfacial charge transfer resistance produced due to the catalyst-electrolyte interaction, solution resistance arising from the migration of the ions in the electrolyte and two parallel circuits composed of resistors and constant phase elements (CPE) respectively. A smaller R_{ct} suggests a quicker charge transfer process meaning better conductivity [37]. The small R_{ct} value of $Cu_{0.005}Co_2P$@EG, mainly due to the presence of conductive EG, alludes to the effective charge transfer from the electrode to the electrolyte validating faster HER kinetics.

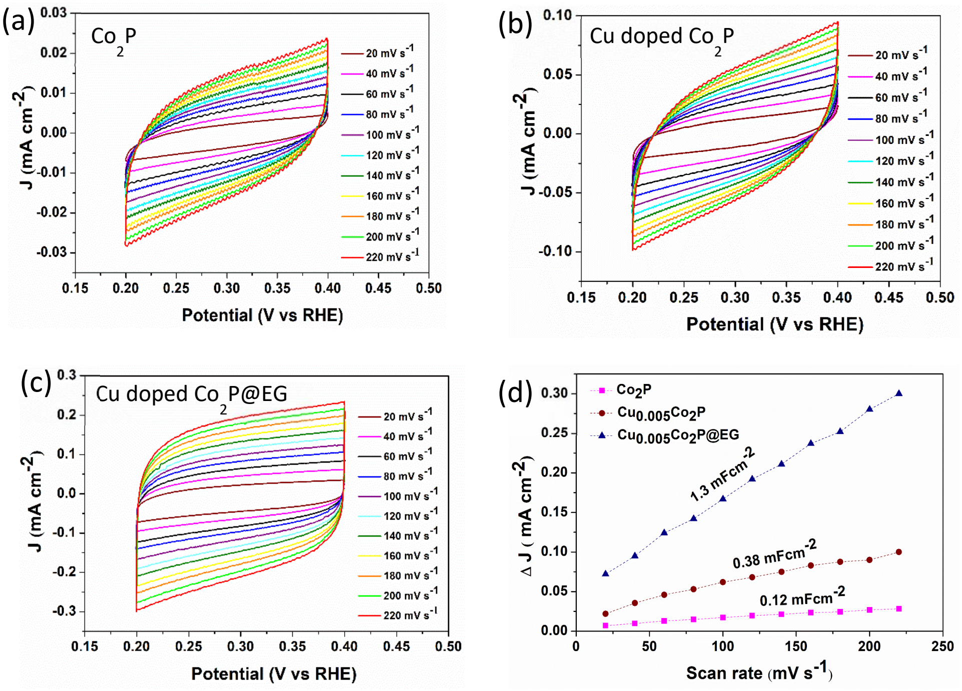

Figure 2.8 Cyclic voltammograms at different scan rate from 20 mV s^{-1} to 220 mV s^{-1} within a non-faradic region for (a) Co$_2$P, (b) Cu$_{0.005}$Co$_2$P, and (c) Cu$_{0.005}$Co$_2$P@EG, (d) Variation of double layer charging current density *vs* scan rate of the synthesized catalysts.

Regarding the remarkable catalytic performance of Cu$_{0.005}$Co$_2$P@EG, the voltammetric analysis was carried out to discern the electrochemical active surface area (ECSA) within the potential range from +0.1 V to +0.3 V with different scan rates where no faradic reaction occurred (**Figure 2.8 (a-c)**). Higher ECSA value signifies more catalytically efficient sites. ECSA was calculated from the electrochemical double-layer capacitance (C_{dl}) that was obtained by fitting the values of the capacitance current (i) and scanning frequency (ν) in equation 2.5.

$$i = \nu C_{dl} \qquad \text{equation 2.5}$$

C_{dl} values calculated for Cu$_{0.005}$Co$_2$P@EG, Cu$_{0.005}$Co$_2$P and Co$_2$P are shown in **Figure 2.8 (d)**. Furthermore, the roughness factor (R_f) was calculated from the C_{dl} values, which is the rate of C_{dl} on 20 μF cm^{-2} (capacitive surface of a smooth electrode) [43]. Measured C_{dl} and R_f values for the catalysts are given in **Table 2.1**.

Table 2.1 Double layer capacitance C_{dl}, roughness factor R_f and electrochemical active surface area ECSA values obtained for different catalysts

Working electrode	***C_{dl}* (mF cm^{-2})**	***R_f* (cm^{-2})**	***ECSA* (cm^2)**
Co_2P	0.12	6	0.42
Cu doped Co_2P	0.38	19	1.33
Cu doped Co_2P@EG	1.3	65	4.55

From these values, it can be proposed that $Cu_{0.005}Co_2P$@EG has a benefit in active surface area (ECSA) and active sites over $Cu_{0.005}Co_2P$ and Co_2P for the improvement of electrocatalytic HER activity.

To further clarify the electron transfer mechanism *via* semiconductor and electrolyte heterojunction, Mott-Schottky (M-S) analysis was carried out. M-S plot deals with parameters like flat band potential (E_{fb}) and charge carrier density (N_D) that is measured from the slope of the M-S graph.

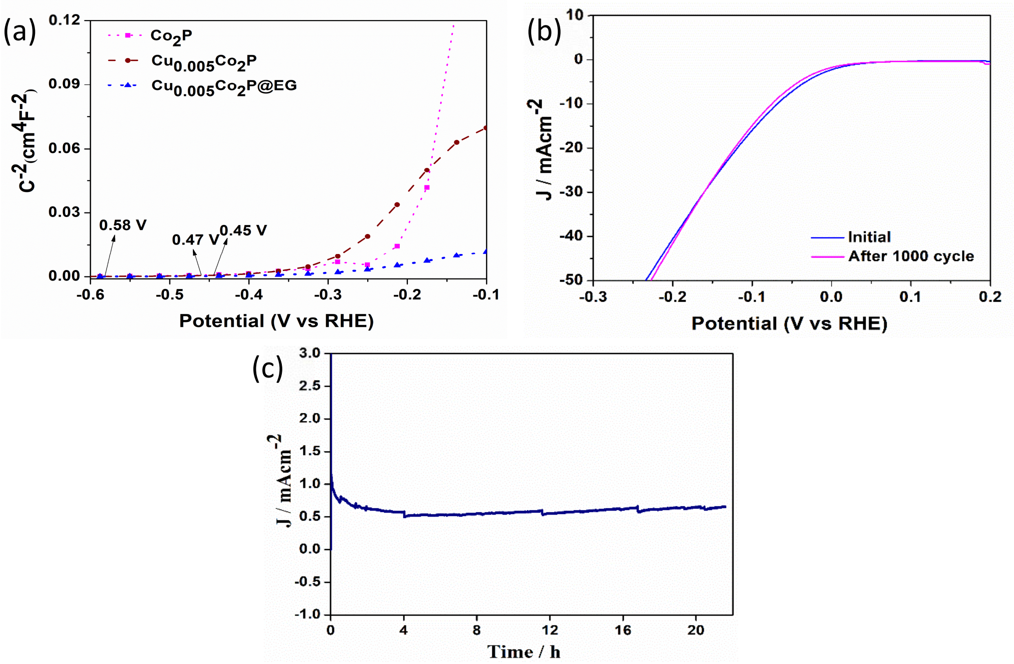

Figure 2.9 (a) M-S plots measured at 0.1 kHz, (b) electrochemical stability of Cu doped Co_2P@EG measured from CV profiles recorded at 50 mV s^{-1} upto 1000 cycles and (c) time dependence study at a specific voltage of 8 mV in 0.5 M H_2SO_4.

After incorporation of Cu doped Co_2P on EG, its charge transfer ability changes due to the difference of valence and conduction band positions. M-S analysis of various catalysts (**Figure 2.9 (a)**) clearly exhibits the positive slope indicating the ntype semi-conductive property of the catalysts and that the carrier is electron [44]. M-S analysis evinces a negative correlation between the slope of the M-S plot and N_D, which implies that smaller the slope greater the charge carrier density. During the contact, the electrode and electrolyte try to attain equilibrium in the potential between their Fermi levels *via* effective charge transfer from one potential region to another thus resulting in band bending. After applying a certain potential, there occurs zero band bending ($1/C_{sc} = 0$), which is known as flat-band potential. N_D and E_{fb} of the catalysts are obtained from the M-S plot using the equations 2.6 (a and b).

$1/C_{SC}^2 = 2\,(E-E_{fb}-K_BT/e)/\,\varepsilon\varepsilon_0\, eN_D$ equation 2.6 (a)

$N_D = 2/\,\varepsilon\varepsilon_0 e\,(\mathrm{d}E/\mathrm{d}(1/C^2))$ equation 2.6 (b)

where C_{SC} is the capacitance of the space charge layer, E is the applied voltage, K_B is the Boltzmann constant (1.38×10^{-23} J K^{-1}), T is the temperature in kelvin (300 K), ε is the dielectric constant of the catalyst, ε_0 is the dielectric constant of free space (8.854×10^{-12} F m^{-1}) and e is the electronic charge (1.603×10^{-19} C) [44,45]. Calculated E_{fb} and N_D values are given in **Table 2.2**.

Table 2.2 Donor density N_D and flat band potential E_{fb} values obtained for different catalysts.

Catalyst	Donor density, N_D ($\times10^{17}$)	E_{fb} (mV)
Co_2P	0.85	0.45
Cu doped Co_2P	2.31	0.47
Cu doped Co_2P@EG	17	0.58

Higher donor density is the reason for higher negative value of E_{fb}. From the calculated values, it is evident that Cu doped Co_2P@EG possesses a higher charge transfer ability than the other catalysts, which approves its greater number of active sites, negligible IR drop and continuous electron transport. These results are in good agreement with the other electrochemical measurements that have been carried out for the catalysts.

The stability of the catalyst Cu doped Co_2P@EG was probed by performing 1000 CV scans within the potential range from 0.1V to -0.3V (*vs* RHE) with a scan rate of 50 mV s^{-1} in 0.5 M H_2SO_4 solution. The integral electrocatalytic performance of the catalyst before and after the stability test suggests the remarkable stability of the catalyst (**Figure 2.9 (b)**). The unique hive like structure of EG likely protects the Cu doped Co_2P nanoparticles from acidic corrosion, thus conserving the catalytic efficiency and exaggerating its industrial application role.

Furthermore, long term functional durability of the catalyst was verified by carrying out chronoamperometric (CA) analysis for ~21.6 h at -60 mV *vs* RHE overpotential. Generally, in acidic electrolyte, the formed H_2 bubbles tend to accumulate on the electrode surface and hence affect the catalytic performance, but such effect was not discerned in our catalyst (due to no current degradation with time) as the present metal phosphide nanoparticles improve the bubble convection that manifests the excellent mass transport property [7]. Initial current degradation in the CA graph is observed which was may be due to adsorbance of proton on the catalyst surface and hence takes time to get stability but the prolonged stable current density after that suggests that Cu doped Co_2P@EG can act as an efficient HER electrocatalyst for a long period (**Figure 2.9 (c)**).

2.3.7 Interpretation of catalytic active site

To interpret the active site in our catalyst Cu doped Co_2P@EG, we checked its catalytic activity with the introduction of conventional thiocyanate ion (SCN^-) in 0.5 M H_2SO_4 solution [46,47]. In acidic conditions, SCN^- could deactivate the metal-centred catalytic sites. In $Cu_{0.005}Co_2P$ a huge potential drop was perceived after infusion of KSCN (5 mM) in the electrolyte (**Figure 2.10 (b)**), but in case of Cu doped Co_2P@EG, only a little change in overpotential was observed with retention of the onset potential (**Figure 2.10 (a)**).

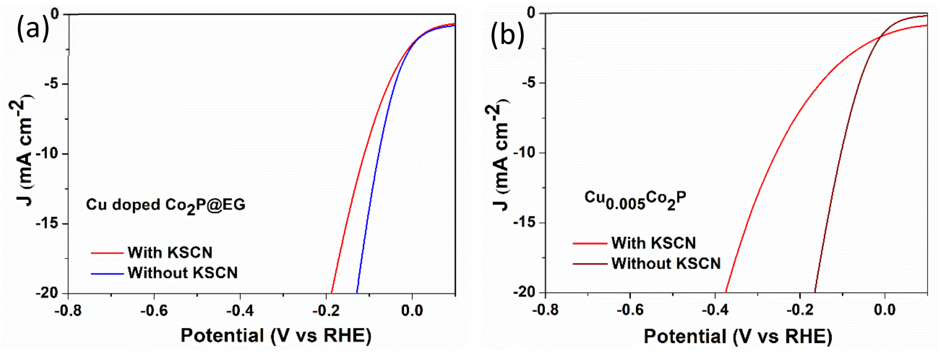

Figure 2.10 HER performances for catalyst (a) $Cu_{0.005}Co_2P$@ EG and (b) $Cu_{0.005}Co_2P$ with and without the addition of KSCN in the electrolyte.

Even though the metal moiety is not the catalytic active site in Cu doped Co_2P@EG, it is a key factor in enhancing the catalytic efficiency and a definite amount of Cu doped Co_2P was masked by SCN^-. Hence SCN^- does affect the catalytic activity of Cu doped Co_2P@EG by bringing a noticeable change in overpotential. Although, the unique hive like structure of EG shields the metal moiety from thiocyanate exposure to some extent but longevity of the catalyst in such an environment can be further improved by encapsulating them within it. However, this survey alluded that in $Cu_{0.005}Co_2P$, metal particles are the sole active sites whereas the HER active sites in Cu doped Co_2P@EG could be primarily the electronically modulated carbon atoms.

2.3.8 Theoretical studies

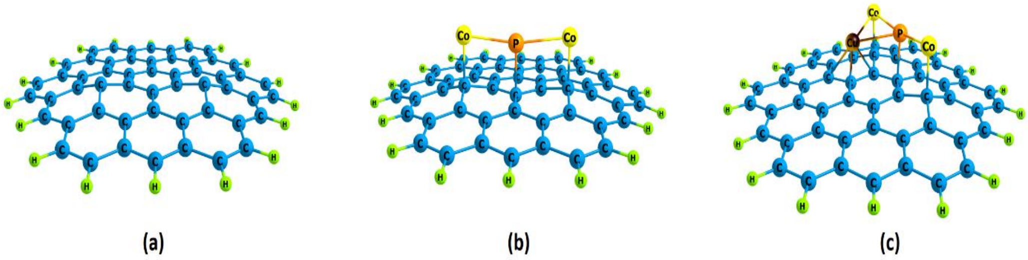

Figure 2.11 Minimum energy structures of (a) EG, (b) Co_2P@EG and (c) Cu doped Co_2P@EG.

For theoretical calculation, we first optimized the geometries of EG, Co_2P@EG, and Cu doped Co_2P@EG (**Figure 2.11**). DFT calculations were performed to discern the insight of the HER activity of EG incorporated Cu doped Co_2P catalyst. Various studies have shown that $\Delta G(H^*)$ is the basic indicator of HER on a broad range of catalytic materials [48]. A catalyst with $\Delta G(H^*) \approx 0$ is considered to be a good candidate for HER [49].

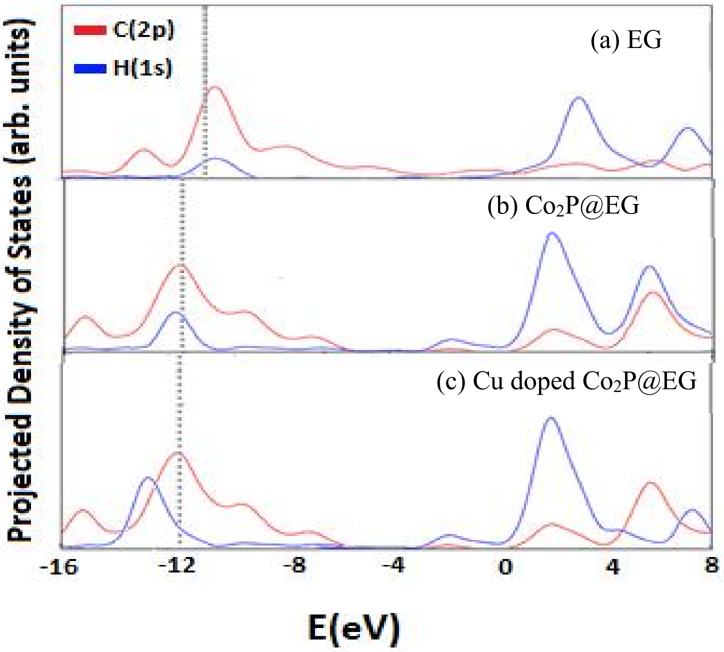

Figure 2.12 Comparison of projected density of states (DOS) of H(1s) and its bonded C(2p) when H is adsorbed on the surface of pristine EG, Co_2P@EG, and Cu doped Co_2P@EG. The dotted lines signify the centre of the occupied band.

Table 2.3 comprises the measured data of ΔG(*H**) on EG, Co_2P@EG and Cu doped Co_2P@EG catalysts. Although the model system assumed in the calculations is smaller in size than that observed experimentally, the required effect can still be acquired by the simple geometry adopted here. ΔG(*H**) on EG is 1.31 eV due to which HER occurs on EG at a large overpotential, which is thermodynamically unfavourable for the formation of the H* intermediate. After the introduction of Co_2P cluster, a notable decrease in ΔG(*H**) value from 1.31 eV to 0.23 eV on EG is obtained. A further significant change is observed with the introduction of Cu in Co_2P cluster as now the linkage of carbon with Co_2P moiety is not only through Co atoms but also the doped Cu atoms due to which ΔG(*H**) reduces to 0.12 eV. This result implies that Cu doping in Co_2P plays a substantial role in adjusting the perfect balance between adsorption-desorption of H_{ads} and thus achieves a much closer to the theoretical value than that of Co_2P@EG.

Table 2.3 Adsorption free energy (**$\Delta G(H^*)$**) for various models **(in eV)**.

Structure	**$\Delta G(H^*)$ in eV**
EG	1.31
Co_2P@EG	0.23
Cu doped Co_2P@EG	0.12

The active carbon site of EG and adsorbed H interacts covalently. The adsorption of H on carbon site of EG is thermodynamically unfavourable due to the inertness of graphite sheet. However, the band centres of the occupied states of C-H bond (sum of C_{2p} and H_{1s}) on both Co_2P@EG and Cu doped Co_2P@EG are located almost in the same lower energy regime than that in pristine EG (**Figure 2.12**). This results stronger C-H_{ads} interaction which delivers HER at a much lower overpotential.

The electrocatalytic performance of the synthesized catalyst is compared towards HER in acidic conditions with other recently documented cobalt phosphide-based catalysts, a table is provided (**Table 2.4**).

Table 2.4 Comparison of activities of different cobalt phosphide-based catalysts towards HER.

Material	Electrolyte	Loading (mg cm^{-2})	Substrate area (cm^2)	Stability	Over-potential (mV)	Tafel slope (mV dec^{-1})	Ref
CoP/CNT	0.05 M H_2SO_4	0.285	N/A	2000 cycles	122	54	[50]
Co_2P nanorod	0.5 M H_2SO_4 & 1M KOH	1.02	0.5	1000 cycles	167 at 0.5M H_2SO_4, 171 at 1M KOH	71, 52	[14]
Co_2P nanoparticles	0.5 M H_2SO_4	1	N/A	500 cycles	95	45	[25]
Co_2P nanowires	0.5 M H_2SO_4	0.17	1	5 h	95	45	[51]
Co_2P@C/CC	0.5 M H_2SO_4	N/A	1	50000 s	100	40.8	[10]
Co_2P@NPG	0.5 M H_2SO_4	0.5	N/A	30 h	103	58	[12]
O–Co_2P	1 M KOH	0.2	0.19	1000 cycles	160	61.1	[11]
CoP/GA	0.5 M H_2SO_4	0.28	N/A	13 h	121	50	[52]
CoP/CNT	0.5 M H_2SO_4	0.285	0.07	18 h	122	54	[53]
CoP NPs/CC	0.5 M H_2SO_4	4	N/A	30 h	48	72	[54]
CoP NS/CC	0.5 M H_2SO_4	10.3	1	40 h	49	30.1	[55]
CoP/CC	0.5 M H_2SO_4	0.92	0.07	80000 s	67	51	[56]
CoP nanotubes	0.5 M H_2SO_4	0.2	0.12	30000 s	129	60	[57]
$Cu_{0.005}Co_2P$@EG	0.5 M H_2SO_4	0.57	0.07	21.6 h	81	113	This work

2.4 Conclusion

In summary, multifaceted Cu doped Co_2P particles on EG layer was fabricated by an easy solvothermal route. Both experimental and theoretical studies approve that the intimate contact of the hollow Cu doped Co_2P particles with EG sheets enhances the charge transfer and also, new energy states emergence activates the carbon site to carry out HER efficiently. The catalyst produces high HER performance with an overpotential of 81 mV at the benchmark current density of 10 mA cm^{-2} with a Tafel slope value of 113 mV dec^{-1} which can be accredited to the specific hollow morphology of the Co_2P along with overall synergistic effect of Cu, Co_2P and EG. This work not only provides an efficient strategy to synthesize both highly active and robust HER electrocatalysts but also looks into how optimized doping content of metal phosphide induced in expanded graphite transforms the inert carbon to an active catalytic site for HER.

2.5 References

[1] Anantharaj, S., Ede, S.R., Sakthikumar, K., Karthick, K., Mishra, S., and Kundu, S. Recent trends and perspectives in electrochemical water splitting with an emphasis on sulfide, selenide, and phosphide catalysts of Fe, Co, and Ni: a review. *Acs Catalysis*, *6*(12):8069-8097, 2016.

[2] Wang, L., Guo, T., Sun, S., Wang, Y., Chen, X., Zhang, K., Zhang, D., Xue, Z., and Zhou, X. Tree-Like NiS 2/MoS 2-RGO Nanocomposites as pH Universal Electrocatalysts for Hydrogen Evolution Reaction. *Catalysis Letters*, *149*:1197-1210, 2019.

[3] Ji, X., Wang, K., Zhang, Y., Sun, H., Zhang, Y., Ma, T., Ma, Z., Hu, P., and Qiu, Y. MoC based Mott–Schottky electrocatalyst for boosting the hydrogen evolution reaction performance. *Sustainable Energy & Fuels*, *4*(1):407-416, 2020.

[4] Huang, G., Liang, W., Wu, Y., Li, J., Jin, Y.Q., Zeng, H., Zhang, H., Xie, F., Chen, J., Wang, N., and Jin, Y. Co_2P/CoP hybrid as a reversible electrocatalyst for hydrogen oxidation/evolution reactions in alkaline medium. *Journal of Catalysis*, *390*:23-29, 2020.

[5] Liu, P. and Rodriguez, J.A. Catalysts for hydrogen evolution from the [NiFe] hydrogenase to the Ni2P (001) surface: the importance of ensemble effect. *Journal of the American Chemical Society*, *127*(42):14871-14878, 2005.

[6] Weng, C.C., Ren, J.T., and Yuan, Z.Y. Transition metal phosphide-based materials for efficient electrochemical hydrogen evolution: a critical review. *ChemSusChem*, *13*(13):3357-3375, 2020.

[7] Wang, J., Liu, Z., Zheng, Y., Cui, L., Yang, W., and Liu, J.Recent advances in cobalt phosphide based materials for energy-related applications. *Journal of Materials Chemistry A*, *5*(44):22913-22932, 2017.

[8] Kucernak, A.R. and Sundaram, V.N.N. Nickel phosphide: the effect of phosphorus content on hydrogen evolution activity and corrosion resistance in acidic medium. *Journal of Materials Chemistry A*, *2*(41):17435-17445, 2014.

[9] Ali, A., Liu, Y., Mo, R., Chen, P., and Shen, P.K. Facile one-step in-situ encapsulation of non-noble metal Co2P nanoparticles embedded into B, N, P tri-doped carbon nanotubes for efficient hydrogen evolution reaction. *International Journal of Hydrogen Energy*, *45*(46):24312-24321, 2020.

[10] Li, C., Gao, H., Wan, W., and Mueller, T. Mechanisms for hydrogen evolution on transition metal phosphide catalysts and a comparison to Pt (111). *Physical Chemistry Chemical Physics*, *21*(44):24489-24498, 2019.

[11] Tan, Y., Wang, H., Liu, P., Cheng, C., Zhu, F., Hirata, A., and Chen, M. 3D nanoporous metal phosphides toward high-efficiency electrochemical hydrogen production. *Advanced Materials*, *28*(15):2951-2955, 2016.

[12] Huang, Z., Chen, Z., Chen, Z., Lv, C., Humphrey, M.G., and Zhang, C. Cobalt phosphide nanorods as an efficient electrocatalyst for the hydrogen evolution reaction. *Nano Energy*, *9*:373-382, 2014.

[13] Ye, C., Wang, M.Q., Chen, G., Deng, Y.H., Li, L.J., Luo, H.Q., and Li, N.B. One-step CVD synthesis of carbon framework wrapped Co 2 P as a flexible electrocatalyst for efficient hydrogen evolution. *Journal of Materials Chemistry A*, *5*(17):7791-7795, 2017.

[14] Xu, K., Ding, H., Zhang, M., Chen, M., Hao, Z., Zhang, L., Wu, C., and Xie, Y. Regulating water-reduction kinetics in cobalt phosphide for enhancing HER catalytic activity in alkaline solution. *Advanced Materials*, *29*(28):1606980, 2017.

[15] Zhuang, M., Ou, X., Dou, Y., Zhang, L., Zhang, Q., Wu, R., Ding, Y., Shao, M., and Luo, Z. Polymer-embedded fabrication of Co2P nanoparticles encapsulated in N, P-doped graphene for hydrogen generation. *Nano letters*, *16*(7):4691-4698, 2016.

[16] Yuan, C.Z., Zhong, S.L., Jiang, Y.F., Yang, Z.K., Zhao, Z.W., Zhao, S.J., Jiang, N., and Xu, A.W. Direct growth of cobalt-rich cobalt phosphide catalysts on cobalt foil: an efficient and self-supported bifunctional electrode for overall water splitting in alkaline media. *Journal of Materials Chemistry A*, *5*(21):10561-10566, 2017.

[17] Fan, M., Cui, J., Wu, J., Vajtai, R., Sun, D., and Ajayan, P.M. Improving the catalytic activity of carbon-supported single atom catalysts by polynary metal or heteroatom doping. *Small*, *16*(22):1906782, 2020.

[18] El-Refaei, S.M., Russo, P.A., and Pinna, N. Recent advances in multimetal and doped transition-metal phosphides for the hydrogen evolution reaction at different pH values. *ACS Applied Materials & Interfaces*, *13*(19):22077-22097, 2021.

[19 Yan, L., Zhang, B., Zhu, J., Li, Y., Tsiakaras, P., and Shen, P.K. Electronic modulation of cobalt phosphide nanosheet arrays via copper doping for highly efficient neutral-pH overall water splitting. *Applied Catalysis B: Environmental*, *265*:118555, 2020.

[20] Lou, X.W., Archer, L.A., and Yang, Z. Hollow micro-/nanostructures: synthesis and applications. *Advanced Materials*, *20*(21):3987-4019, 2008.

[21] Xia, X., Wang, Y., Ruditskiy, A., and Xia, Y. 25th anniversary article: galvanic replacement: a simple and versatile route to hollow nanostructures with tunable and well-controlled properties. *Advanced Materials*, *25*(44):6313-6333, 2013.

[22] Yu, L., Wu, H.B., and Lou, X.W.D. Self-templated formation of hollow structures for electrochemical energy applications. *Accounts of chemical research*, *50*(2):293-301, 2017.

[23] Callejas, J.F., Read, C.G., Popczun, E.J., McEnaney, J.M., and Schaak, R.E. Nanostructured Co_2P electrocatalyst for the hydrogen evolution reaction and direct comparison with morphologically equivalent CoP. *Chemistry of Materials*, *27*(10):3769-3774, 2015.

[24] Li, Z., Wu, D., Ouyang, Y., Wu, H., Jiang, M., Wang, F., and Zhang, L.Y. Synthesis of hollow cobalt phosphide nanocrystals with ultrathin shells anchored on reduced graphene oxide as an electrocatalyst toward hydrogen evolution. *Applied Surface Science*, *506*:144975, 2020.

[25] Gong, K., Du, F., Xia, Z., Durstock, M., and Dai, L. Nitrogen-doped carbon nanotube arrays with high electrocatalytic activity for oxygen reduction. *science*, *323*(5915):760-764, 2009.

[26] Zou, X., Huang, X., Goswami, A., Silva, R., Sathe, B.R., Mikmeková, E., and Asefa, T. Cobalt-embedded nitrogen-rich carbon nanotubes efficiently catalyze hydrogen evolution reaction at all pH values. *Angewandte Chemie*, *126*(17):4461-4465, 2014.

[27] Deng, J., Ren, P., Deng, D., Yu, L., Yang, F., and Bao, X. Highly active and durable non-precious-metal catalysts encapsulated in carbon nanotubes for hydrogen evolution reaction. *Energy & Environmental Science*, *7*(6):1919-1923, 2014.

[28] Zheng, W. and Wong, S.C. Electrical conductivity and dielectric properties of PMMA/expanded graphite composites. *Composites Science and Technology*, *63*(2):225-235, 2003.

[29] Perdew, J.P., Burke, K., and Ernzerhof, M. Generalized gradient approximation made simple. *Physical review letters*, *77*(18):3865, 1996.

[30] M. E. Frisch, G. W. Trucks, H. B. Schlegel, G. E. Scuseria, M. A. Robb, J. R. Cheeseman, ...; D. J. Fox, Gaussian 16 (2016).

[31] Lu, T. and Chen, F. Multiwfn: A multifunctional wavefunction analyzer. *Journal of computational chemistry*, *33*(5):580-592, 2012.

[32] Hatui, G., Malas, A., Bhattacharya, P., Dhibar, S., Kundu, M.K., and Das, C.K. Effect of expanded graphite and PEI-co-Silicon Rubber on the thermo mechanical, morphological as well as rheological properties of in situ composites based on poly (ether imide) and liquid crystalline polymer. *Journal of Alloys and Compounds*, *619*:709-718, 2015.

[33] Pan, Y., Liu, Y., Lin, Y., and Liu, C. Metal doping effect of the M–Co2P/Nitrogen-Doped carbon nanotubes (M= Fe, Ni, Cu) hydrogen evolution hybrid catalysts. *ACS applied materials & interfaces*, *8*(22):13890-13901, 2016.

[34] Güler, Ö., Güler, S.H., Selen, V., Albayrak, M.G., and Evin, E. Production of graphene layer by liquid-phase exfoliation with low sonication power and sonication time from synthesized expanded graphite. *Fullerenes, Nanotubes and Carbon Nanostructures*, *24*(2):123-127, 2016.

[35] Wang, J., Johnston-Peck, A.C., and Tracy, J.B. Nickel phosphide nanoparticles with hollow, solid, and amorphous structures. *Chemistry of Materials*, *21*(19), pp.4462-4467. [36] Liu, X., Deng, S., Liu, P., Liang, J., Gong, M., Lai, C., Lu, Y., Zhao, T. and Wang, D., 2019. Facile self-template fabrication of hierarchical nickel-cobalt phosphide hollow nanoflowers with enhanced hydrogen generation performance. *Science Bulletin*, *64*(22):1675-1684, 2009.

[37] Wei, B. and Yang, S. Polymer composites with expanded graphite network with superior thermal conductivity and electromagnetic interference shielding performance. *Chemical Engineering Journal*, *404*:126437, 2021.

[38] Yagi, Y., Briere, T.M., Sluiter, M.H., Kumar, V., Farajian, A.A., and Kawazoe, Y. Stable geometries and magnetic properties of single-walled carbon nanotubes doped with 3 d transition metals: A first-principles study. *Physical Review B*, *69*(7):075414, 2004.

[39] Ge, R., Huo, J., Liao, T., Liu, Y., Zhu, M., Li, Y., Zhang, J., and Li, W. Hierarchical molybdenum phosphide coupled with carbon as a whole pH-range electrocatalyst for hydrogen evolution reaction. *Applied Catalysis B: Environmental*, *260*:118196, 2020.

[40] Liu, Z., Ai, J., Sun, M., Han, F., Li, Z., Peng, Q., Wang, Q.D., Liu, J., and Liu, L. Phosphorous-Doped Graphite Layers with Outstanding Electrocatalytic Activities for the Oxygen and Hydrogen Evolution Reactions in Water Electrolysis. *Advanced Functional Materials*, *30*(12):1910741, 2020.

[41] Lotfi, N., Shahrabi, T., Yaghoubinezhad, Y., and Darband, G.B. Electrodeposition of cedar leaf-like graphene Oxide@ Ni–Cu@ Ni foam electrode as a highly efficient and ultra-stable catalyst for hydrogen evolution reaction. *Electrochimica Acta*, *326*:134949, 2019.

[42] Liao, L., Wang, S., Xiao, J., Bian, X., Zhang, Y., Scanlon, M.D., Hu, X., Tang, Y., Liu, B., and Girault, H.H. A nanoporous molybdenum carbide nanowire as an electrocatalyst for hydrogen evolution reaction. *Energy & environmental science*, *7*(1):387-392, 2014.

[43] Gao, D., Guo, J., Cui, X., Yang, L., Yang, Y., He, H., Xiao, P., and Zhang, Y. Three-dimensional dendritic structures of NiCoMo as efficient electrocatalysts for the hydrogen evolution reaction. *ACS Applied Materials & Interfaces*, *9*(27):22420-22431, 2017.

[44] Fabregat-Santiago, F., Garcia-Belmonte, G., Bisquert, J., Bogdanoff, P., and Zaban, A., Mott-Schottky analysis of nanoporous semiconductor electrodes in dielectric state deposited on SnO_2 (F) conducting substrates. *Journal of the Electrochemical Society*, *150*(6):E293, 2003.

[45] Darowicki, K., Krakowiak, S., and Ślepski, P. Selection of measurement frequency in Mott–Schottky analysis of passive layer on nickel. *Electrochimica Acta*, *51*(11):2204-2208, 2006.

[46] Yang, F., Chen, Y., Cheng, G., Chen, S., and Luo, W. Ultrathin nitrogen-doped carbon coated with CoP for efficient hydrogen evolution. *ACS Catalysis*, *7*(6):3824-3831, 2017.

[47] Yang, Y., Liang, X., Li, F., Li, S., Li, X., Gao, W., Tang, Y., Ng, S., Wu, C.L., and Li, R. Encapsulating Co_2P@ C Core-Shell Nanoparticles in Porous Carbon Sandwich: a Nitrogen and Phosphorus Dual-Doped PH-Universal Electrocatalysts for High-efficient Hydrogen Evolution. *ChemSusChem*, *11*:376-388, 2018.

[48] Hinnemann, B., Moses, P.G., Bonde, J., Jørgensen, K.P., Nielsen, J.H., Horch, S., Chorkendorff, I., and Nørskov, J.K. Biomimetic hydrogen evolution: MoS2 nanoparticles as catalyst for hydrogen evolution. *Journal of the American Chemical Society*, *127*(15):5308-5309, 2005.

[49] Nørskov, J.K., Bligaard, T., Logadottir, A., Kitchin, J.R., Chen, J.G., Pandelov, S., and Stimming, U. Trends in the exchange current for hydrogen evolution. *Journal of The Electrochemical Society*, *152*(3):J23, 2005.

[50] Liu, Q., Tian, J., Cui, W., Jiang, P., Cheng, N., Asiri, A.M., and Sun, X. Carbon nanotubes decorated with CoP nanocrystals: a highly active non-noble-metal nanohybrid electrocatalyst for hydrogen evolution. *Angewandte Chemie International Edition*, *53*(26):6710-6714, 2014.

[51] Jin, Z., Li, P., and Xiao, D. Metallic Co_2P ultrathin nanowires distinguished from CoP as robust electrocatalysts for overall water-splitting. *Green Chemistry*, *18*(6):1459-1464, 2016.

[52] Zhang, X., Han, Y., Huang, L., and Dong, S. 3D graphene aerogels decorated with cobalt phosphide nanoparticles as electrocatalysts for the hydrogen evolution reaction. *ChemSusChem*, *9*(21):3049-3053, 2016.

[53] Liu, Q., Tian, J., Cui, W., Jiang, P., Cheng, N., Asiri, A.M., and Sun, X. Carbon nanotubes decorated with CoP nanocrystals: a highly active non-noble-metal nanohybrid electrocatalyst for hydrogen evolution. *Angewandte Chemie International Edition*, *53*(26):6710-6714, 2014.

[54] Li, Q., Xing, Z., Asiri, A.M., Jiang, P., and Sun, X. Cobalt phosphide nanoparticles film growth on carbon cloth: a high-performance cathode for electrochemical hydrogen evolution. *International journal of hydrogen energy*, *39*(30):16806-16811, 2014.

[55] Yang, X., Lu, A.Y., Zhu, Y., Hedhili, M.N., Min, S., Huang, K.W., Han, Y., and Li, L.J. CoP nanosheet assembly grown on carbon cloth: A highly efficient electrocatalyst for hydrogen generation. *Nano Energy*, *15*:634-641, 2015.

[56] Tian, J., Liu, Q., Asiri, A.M., and Sun, X. Self-supported nanoporous cobalt phosphide nanowire arrays: an efficient 3D hydrogen-evolving cathode over the wide range of pH 0–14. *Journal of the American Chemical Society*, *136*(21):7587-7590, 2014.

[57] Du, H., Liu, Q., Cheng, N., Asiri, A.M., Sun, X., and Li, C.M. Template-assisted synthesis of CoP nanotubes to efficiently catalyze hydrogen-evolving reaction. *Journal of Materials Chemistry A*, *2*(36):14812-14816, 2014.